Harmonic moment dynamics in Laplacian growth

Alexander Leshchiner,[1] Matthew Thrasher,[1] Mark B. Mineev-Weinstein,[2] and Harry L. Swinney[1,*]
[1]*Center for Nonlinear Dynamics and Physics Department, University of Texas at Austin, Austin, Texas 78712, USA*
[2]*Applied Physics Division, MS-P365, Los Alamos National Laboratory, Los Alamos, New Mexico 87545, USA*
(Received 30 January 2009; revised manuscript received 12 November 2009; published 12 January 2010)

Harmonic moments are integrals of integer powers of $z=x+iy$ over a domain. Here, the domain is an exterior of a bubble of air growing in an oil layer between two horizontal closely spaced plates. Harmonic moments are a natural basis for such Laplacian growth phenomena because, unlike other representations, these moments linearize the zero surface tension problem [S. Richardson, J. Fluid Mech. **56**, 609 (1972)], so that all moments except the lowest one (the area of the bubble) are conserved in time. In our experiments, we directly determine the harmonic moments and show that for nonzero surface tension, all moments (except the lowest one) decay in time rather than exhibiting the divergences of other representations. Further, we derive an expression that relates the derivative of the k^{th} harmonic moment M_k to measurable quantities (surface tension, viscosity, the distance between the plates, and a line integral over the contour encompassing the growing bubble). The laboratory observations are in good accord with the expression we derive for dM_k/dt, which is proportional to the surface tension; thus in the zero surface tension limit, the moments (above $k=0$) are all conserved, in accord with Richardson's theory. In addition, from the measurements of the time evolution of the harmonic moments we obtain a value for the surface tension that is within 20% of the accepted value. In conclusion, our analysis and laboratory observations demonstrate that an interface dynamics description in terms of harmonic moments is physically realizable and robust.

DOI: 10.1103/PhysRevE.81.016206 PACS number(s): 47.54.−r, 47.20.Ma, 47.15.gp, 02.30.Ik

I. INTRODUCTION

A. Laplacian growth and viscous fingering

Nonequilibrium processes give rise to a variety of patterns with remarkable geometrical and dynamical properties [1,2]. Often these processes are represented by the dynamics of an unstable interface between different phases, and the interface patterns can exhibit universal features [3]. Examples include crack propagation [2], fluid-fluid interface dynamics [4], crystal formation [5], and biological growth [6].

The simplest process leading to unstable universal patterns is *Laplacian growth*, where the velocity of an interface is proportional to the gradient of function that is harmonic outside (or inside) the interface. Here, we examine the simplest example of Laplacian growth, quasi-two-dimensional (2D) viscous fingering in a Hele-Shaw cell [7], where a viscous fluid is displaced by an inviscid fluid between two horizontal closely spaced parallel plates.

Figure 1 shows four viscous fingering patterns grown in the radial Hele-Shaw cell described in Sec. IV. Viscous silicone oil is removed from a buffer surrounding the plates and air enters between the plates through a central hole in the bottom plate.

As the air bubble expands, the oil/air interface is unstable. The depth averaged velocity $\mathbf{v}(x,y)$ and the pressure $p(x,y)$ in the oil are approximated by Darcy's law [8],

$$\mathbf{v} = -\frac{b^2}{12\mu}\nabla p, \tag{1}$$

where b is the spacing between the plates and μ is the dynamic oil viscosity. The oil is incompressible, so div $\mathbf{v}=0$. From Eq. (1) it then follows that in the oil,

$$\nabla^2 p = 0. \tag{2}$$

Since the normal velocities of the interface V and of the fluid at the interface coincide [8],

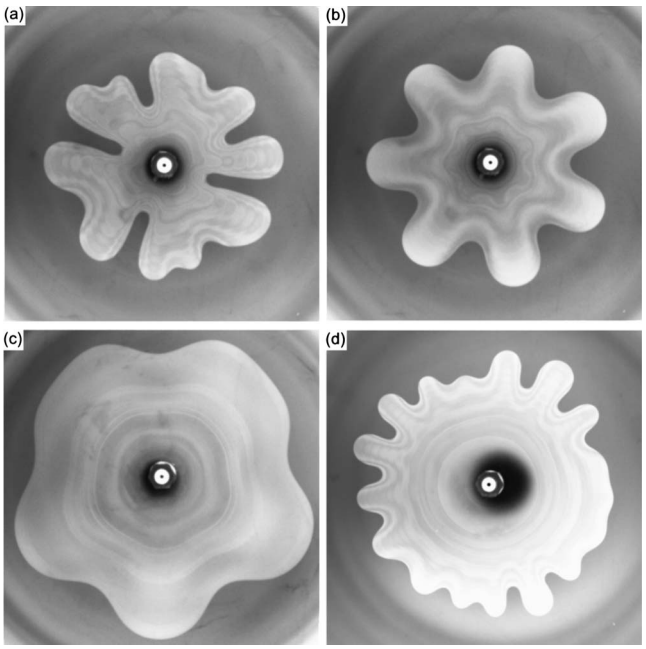

FIG. 1. Viscous fingering patterns of air in oil contained between two plates separated by 125 μm (image size is 14 cm $\times$14 cm). (a) Bubble grown at a constant pumping rate of 0.52 mL/min. (b), (c), (d) Bubbles grown with varying pumping rates, as described in Sec. IV B. The time development of bubble (b) is shown in Fig. 3.

*swinney@chaos.utexas.edu

$$V = -\frac{b^2}{12\mu}\partial_n p, \tag{3}$$

where ∂_n is the normal component of the gradient. Because the air is nearly inviscid, the pressure in the air is essentially uniform, and its value can be taken as zero. Thus, the pressure jump across the oil/air interface coincides with the oil pressure at the interface and is given by [4]

$$p = -\sigma\kappa, \tag{4}$$

where σ is surface tension and κ is the local curvature of the interface in the horizontal plane. An updated boundary condition including a $\pi/4$ multiplicative factor and an additional term correcting for wetting will be presented in Sec. III B.

The asymptotic pressure boundary condition in oil far from the interface in the radial geometry is

$$p = -\frac{3\mu Q}{\pi b^2}\log(x^2+y^2) \quad (\text{for } x^2+y^2 \to \infty), \tag{5}$$

where Q is the pumping rate (the rate of area growth), which may depend on time. Equations (1)–(5) complete the description of 2D viscous fingering, which is a prototype of Laplacian growth.

Laplacian growth, a classical free-boundary problem [9], is famous in physics becasue the process is highly unstable, dissipative, non-equilibrium, and nonlinear, and because the growth produces universal patterns [4,10,11]. Laplacian growth is also famous in mathematics, because the description Eqs. (1)–(5), as simple as it looks, reveals a powerful and profound structure [12–14]

Laplacian growth occurs in many physical systems and is known by names such as crystal growth, amorphous solidification [5], electrodeposition [15,16], bacterial colony growth [6], diffusion-limited aggregation (DLA) [17], motion of a charged surface in liquid helium [18], and viscous fingering [19]. There are thousands of articles (theoretical, experimental, and computational) devoted to Laplacian growth if one includes work on closely connected problems such as the Stefan problem (solidification) [20,21], DLA [22], and the phase-field model [2]. Nevertheless, many features remain unexplained, despite extensive effort and full knowledge of the laws of physics describing the process.

B. Harmonic moments

The present work concerns a powerful description of Laplacian growth called *harmonic moments*. Our work demonstrates that robust results for the time evolution of harmonic moments can be obtained from viscous fingering data. Harmonic moments are defined as

$$M_k = \int_D z^{-k}\frac{dxdy}{\pi} = -\oint_\Gamma z^{-k}\bar{z}\frac{dz}{2\pi i}, \tag{6}$$

where $k=0,1,\ldots,\infty$, $z=x+iy$, and the domain of integration D is *exterior* to a pattern's boundary Γ and bounded by a large circle on the outside. These are exterior moments, which are relevant for exterior Laplacian growth, when a viscous fluid is outside the interface, as in this work. Interior moments, which are relevant for interior Laplacian growth when a viscous fluid is inside the interface, are defined similarly, but with positive powers of z under the integral, which is taken over the interior of the pattern.

Harmonic moments are of fundamental importance for Laplacian growth because in the absence of surface tension, there is an infinite number of conservation laws, all moments M_k (except for $k=0$) are *conserved in time*, as was discovered by Richardson (1972) [23] for the interior Laplacian growth problem. The conservation laws have been extended to the exterior case [24] and are experimentally confirmed in this work. In the harmonic moments basis, the whole evolution of $D(t)$ is reduced to the time-dependent area of a growing bubble, which is $M_0(t)$. This result selects the "harmonic basis" M_k from all other bases as the best basis for describing $D(t)$ in Laplacian growth.

Harmonic moments form a complete basis for representing any 2D interface, regardless of its complicated shape, provided that D is analytic and singly connected [25,26]. Like Fourier modes, each harmonic moment M_k corresponds to a particular aspect of the interface. The moment M_0 is the area of the domain D divided by π. Moments M_k for $k \geq 1$ are proportional to the amplitude of a monochromatic wave, which modulates the circle with an exactly k waves along the circumference,

$$z = R\exp(i\phi)[1 + a_k \exp(-ik\phi)],$$

where ϕ is a "stream function" parameter along the interface, a_k is an amplitude, and R is the bubble radius. Specifically, $M_k = a_k R^{2-k}$. For an approximately n-fold pattern, the dominant moments are M_n, M_{2n}, M_{3n}, etc. [e.g., Figure 1(b) is approximately sevenfold symmetric and Fig. 1(c) is approximately fivefold symmetric]. However, care should be taken in comparing different moments since they have different units; the moment M_k has units cm^{2-k}.

Viscous fingering structures become extremely complex for high-growth rates, where tips repeatedly split and form new fingers and fjords. Hence, it is remarkable that theory predicts that a set of purely geometrical quantities, M_k, will change slowly during the growth process and will have a well-defined limit as the surface tension approaches zero. The unique properties of harmonic moments have been already used to establish connections between Laplacian growth and other fields of physics and mathematics [12–14], but no previous studies have attempted to extract harmonic moments from laboratory data. Our work demonstrates that robust moments M_k can indeed be obtained from experiments, and particularly that the moments M_k for $k \geq 1$ are conserved in the limit of zero surface tension.

C. Overview

In the following section, we present some additional properties of harmonic moments. Sec. III extends the theory for harmonic moments in viscous fingering to the physical case, where the surface tension is not zero. In this case, the moments M_k with positive k are no longer conserved, but their time derivatives are proportional to surface tension and, hence, vanish in the zero surface tension limit. Section IV

presents our experimental and data analysis methods. Section V presents results for harmonic moments determined from experiments for a wide range of conditions. Also we show that the results for the harmonic moments can be used to deduce a physical parameter, such as surface tension. Section VI discusses the significance of our results.

II. HARMONIC MOMENTS: HISTORY AND APPLICATIONS

A. Inverse potential problem

The origin of harmonic moments dates back to Isaac Newton's study of the inverse potential problem, which was subsequently investigated by Kelvin, Poincaré, and many researchers in the twentieth century. The inverse potential problem [25,26] asks how to recover the shape of a domain occupied by a uniformly distributed mass, given the gravitational potential created by this mass outside the domain. Surprisingly, this classical mathematical problem was found to be at the heart of the underlying mathematical structure of Laplacian growth [12–14,23]. In two dimensions the gravitational potential created by uniformly distributed mass (with unit density) occupying the domain D is given by

$$\Phi(x,y) = \frac{1}{\pi}\int_D \log|z-z'|dx'dy'$$

$$= \frac{1}{\pi}\int_D \log|z'|dx'dy' - \mathcal{R}e\sum_{k=1}^{\infty} M_k z^k/k, \qquad (7)$$

if z and the origin lie outside D. The M_k, defined in Eq. (6), are multipole moments of the mass distribution [27]. In Laplacian growth the M_k are traditionally called harmonic moments. In Eq. (6) the moments M_k are defined for a radial geometry. For a rectangular geometry, where matter occupies a horizontal semi-infinite strip D with a width L bounded from the left by an arbitrary curve, and periodically extended (repeated) both up and down infinitely, the moments are defined as $M_k = \int_D \exp(-2\pi k z/L)dxdy/\pi$. This geometry is relevant for Laplacian growth in a rectangular Hele-Shaw channel, which has been studied since the work by Saffman and Taylor [4].

B. Connections and applications

In science and engineering it is often of interest to find the shape of an object from the indirect measurement of the harmonic moments M_k. The problem of domain reconstruction from its moments has applications in many areas, including signal processing, probability and statistics, tomography, and the inverse potential problem in geophysics (magnetic and gravitational anomaly detection) [28]. While the recovery of shapes from moments is often an ill-posed problem, it was recently recognized that the moments problem allows the complete closed form solution for so-called quadrature domains [29], a branch of mathematics created in 1970s [30,31]. Remarkably, these solutions are based on a technique of numerical *linear* algebra that yields numerically stable and fast algorithms and exposes a deep connection between harmonic moments and a theory of analytic approximation [32,33].

III. THEORY OF HARMONIC MOMENTS WITH NONZERO SURFACE TENSION

A. Derivation of dM_k/dt

In Laplacian growth with nonzero surface tension the harmonic moments are no longer conserved. To relate the dynamics of the harmonic moments to measurable quantities in viscous fingering, we now obtain an expression for the time derivative of the harmonic moments in terms of a line integral over the air/oil interface. The time derivative of M_k follows from the definition (1) and (6), $\frac{dM_k}{dt} = \frac{b^2}{12\mu}\oint_\Gamma z^{-k}\partial_n p \frac{dl}{\pi} =$.

We want to exchange the derivative between p and z^{-k}, so we add and subtract $p\partial_n z^{-k}$ from the integrand,

$$= \frac{b^2}{12\mu}\oint_\Gamma (z^{-k}\partial_n p - p\partial_n z^{-k} + p\partial_n z^{-k})\frac{dl}{\pi}. \qquad (8)$$

Here l is the arc length along the interface Γ. The integral of the first two terms is zero by Gauss' theorem, after using Eq. (3) and the analyticity of z^{-k} in D,

$$\oint_\Gamma (z^{-k}\partial_n p - p\partial_n z^{-k})dl = \oint_\Gamma (z^{-k}\nabla p - p\nabla z^{-k})\cdot \vec{n}dl$$

$$= \int_D \nabla\cdot(z^{-k}\nabla p - p\nabla z^{-k})dxdy = 0. \qquad (9)$$

Using Eq. (4) for the pressure, we have

$$\frac{dM_k}{dt} = -\frac{\sigma b^2}{12\pi\mu}\oint_\Gamma \kappa\partial_n z^{-k}dl, \qquad (10)$$

with the interfacial curvature given by $\kappa = d\theta/dl$, where θ is the angle of a tangent line to the interface. Using the identity $\partial_n z^{-k} = i\partial_l z^{-k} = -ikz^{-(k+1)}dz/dl$, where ∂_l denotes a tangential derivative, we have,

$$-\frac{\sigma b^2 i}{12\pi\mu}\oint_\Gamma \frac{d\theta}{dl}\partial_l z^{-k}dl = \frac{k\sigma b^2 i}{12\pi\mu}\oint_\Gamma z^{-(k+1)}\frac{dz}{dl}d\theta$$

$$= \frac{k\sigma b^2}{12\pi\mu}\oint_\Gamma z^{-(k+1)}de^{i\theta}, \qquad (11)$$

where the last expression was obtained using $dz/dl = \exp(i\theta)$. Integrating by parts, we obtain,

$$\frac{dM_k}{dt} = \sigma k(k+1)\frac{b^2}{12\pi\mu}\oint_\Gamma e^{i\theta}\frac{dz}{z^{k+2}}. \qquad (12)$$

This new result relates a measurable property, the time derivative of the harmonic moment M_k, to a measurable line integral (over a growing bubble) and measurable physical properties (the surface tension σ, viscosity μ, and plate spacing b). Equation (12) in the limit that the surface tension vanishes recovers Richardson's result for the conservation of moments. Surface tension is in this context a regular rather

than singular perturbation. The prediction of Eq. (12), modified to include the affect of wetting as described in the next subsection, is tested in Sec. V B.

B. Wetting and scaling correction

The pressure jump at the interface Eq. (4) must be modified because as the air bubble advances between the glass plates, it leaves behind a wetting film on each plate. The thickness of this film increases with the interface's velocity [34]. This film can be seen as interference fringes on the images in Fig. 1, because the interface is slowing down as the bubble expands. In addition, a factor $\pi/4$ is needed in Eq. (4). The pressure jump including the wetting correction and a factor $\pi/4$ [not in Eq. (4)] was calculated by Park and Homsy to be [34],

$$p = -\sigma\left(\frac{\pi\kappa}{4}\right) + \frac{2\sigma}{b}\left[1 + 3.8\left(\frac{\mu V}{\sigma}\right)^{2/3}\right], \tag{13}$$

where V is the local normal velocity of the interface. The thickness of the film predicted by Park and Homsy was experimentally confirmed by Tabeling and Libchaber [35] for $6\times10^{-4} < \frac{\mu V}{\sigma} < 3\times10^{-3}$.

The interface velocity V is greatest at the finger tips and is much smaller at the sides of the fingers. Conventionally the base of the fjord is called a stagnation point, although in these experiments there is small motion at the base of the fjords as a consequence of relaxation due to surface tension; the base of the fjord becomes more bulbous the longer surface tension has acted on it.

After substituting this new expression (13) for the pressure jump into Eq. (10), we obtain,

$$\frac{dM_k}{dt} = \sigma k \frac{b^2\pi}{12\mu}\left[\frac{k+1}{4}\oint_\Gamma e^{i\theta}\frac{dz}{z^{k+2}} + \frac{3.8i}{\pi b/2}\oint_\Gamma\left(\frac{\mu V}{\sigma}\right)^{2/3}\frac{dz}{z^{k+1}}\right]. \tag{14}$$

C. Testing the theory and determination of surface tension

In Sec. V we compute the moments $M_k(t)$ for growing viscous fingering patterns directly from the pattern geometry using the definition Eq. (6). The time evolution of the moments can be compared to the result in the zero surface tension limit, where the moments are conserved. We will also compare different moments by computing the normalized amplitudes,

$$a_k = |M_k|/|M_0|^{2/(2-k)}. \tag{15}$$

Further, we can directly test the theory using Eq. (14) and measuring the time derivative of the moments and independently determining,

(i) the fluid surface tension σ,

(ii) the fluid viscosity μ,

(iii) the thickness b of the gap between the plates,

(iv) the interface velocity V in the second integral in Eq. (14) (this can be obtained from analysis of images of the air bubble as a function of time, described in Sec. IV D), and

(v) the two integrals in Eq. (14).

Alternatively, we can use the theory to determine a fluid property if the other four quantities are independently known. This is the way in which we determine the surface tension in Sec. V. However, since numerical differentiation of the data for $M_k(t)$ is difficult to do accurately, we take one more step to obtain a working equation with improved signal to noise: Eq. (14) is integrated over a time interval to obtain,

$$M_k(t_2) - M_k(t_1) = \sigma k\frac{b^2}{48\mu}(k+1)\int_{t_1}^{t_2}\oint_\Gamma e^{i\theta}\frac{dz}{z^{k+2}}dt + \sigma k\frac{b^2}{12\mu\pi}\int_{t_1}^{t_2}\frac{3.8i}{b/2}\oint_\Gamma\left(\frac{\mu V}{\sigma}\right)^{2/3}\frac{dz}{z^{k+1}}dt. \tag{16}$$

With only the definition of moments Eq. (6), the dynamics cannot be related to known physical quantities. However, with Eq. (16), the dynamics can be quantitatively connected to known physical quantities. Equation (16) is a cubic equation of the form $a\sigma + b\sigma^{1/3} + c = 0$, where a, b, and c are complex numbers. We solve this equation numerically in Sec. V B to deduce the surface tension and to test the predicted decay rates of the moments.

IV. EXPERIMENT

A. Apparatus

An oil layer is contained in a Hele-Shaw cell consisting of two horizontal, closely spaced glass plates with a hole through the center of the bottom plate. When oil is pumped out of a buffer that surrounds the oil layer, air (at nearly atmospheric pressure) enters the layer through the hole in the bottom plate and forms a bubble in the center of the oil layer.

The optically polished glass plates each have diameter 28.8 cm and thickness 6.0 cm; each plate is flat to 0.2 μm, as described in [10,19]. The gap between the plates was either 125 ± 5 μm or 384 ± 6 μm; most of the gap uncertainty arises from using a micrometer to measure the thickness of the metal shims that set the size of the gap. Interferometric measurements using a sodium lamp showed that the gap thickness was uniform to 0.3 μm for the 125 μm gap and 1.6 μm for the 384 μm gap.

The oil was Dow Corning 200 silicone oil at 24 °C. We measured the viscosity $\mu = 49.9\pm0.3$ mPa s with a Paar Physica MCR300 rheometer. The surface tension $\sigma_{reference} = 21.1\pm0.1$ mN/m was measured by the Wilhelmy Plate method using a Kruss K11 tensiometer. The density was measured to be $\rho = 0.9585\pm0.0005$ g/cm^3.

Bubble patterns were imaged from above with a CCD camera (1300×1030 pixels). The frame rate ranged from 1/6 to 2 frames/s, depending on the growth rate of a bubble.

B. Growth of a bubble

Experiments were initiated by obtaining a nearly circular air bubble, grown by slowly withdrawing oil from the buffer surrounding the gap between the plates. After an initial nearly circular bubble had been grown to a radius of at least

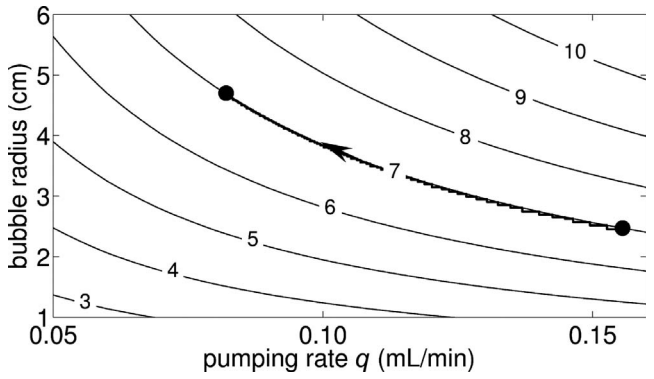

FIG. 2. In order to grow an approximately n-fold symmetric bubble, the pumping rate is adjusted to follow Eq. (17), as illustrated here by curves for different n. The sevenfold bubble in Fig. 1(b) was grown in this way, as indicated by the bold line. We measure the area of a growing bubble in real time from the video images, and compute from that area a radius for a circle with that area. Then, given a target n-fold symmetry, the pumping rate is adjusted (in small steps) to stay on the desired n-fold curve of the graph. These curves apply to a cell with gap thickness of 125 μm.

2 cm (to give good spatial resolution in the images), multifingered bubbles like those in Fig. 1 were grown by using a precision computer-controlled syringe pump to remove oil from the annular buffer at a specified rate. Growth of a full-sized bubble (15–20 cm diameter) took from 30 to 1600 s (typically 300 s).

After obtaining a nearly circular bubble, a multifingered bubble can be obtained by pumping oil out of the buffer. Usually fluid is removed at a fixed rate, as in our laboratory's previous viscous fingering experiments [10,19]. However, with a fixed pumping rate, the n-fold mode that is the fastest growing changes with time, and the resultant bubble has many azimuthal modes with a substantial amplitude [e.g., Figure 1(d)].

Our procedure for obtaining the harmonic moments and deducing the surface tension is applicable for bubbles grown with *any* pumping rate, $q(t)=bQ(t)$. However, results for the harmonic moments are more robust if a bubble retains an approximate n-fold symmetry as it grows. To achieve this, the pumping rate must decrease in a way that maintains an approximate n-fold symmetry. A linear stability analysis by Bataille [36,37] provides an expression for the pumping rate needed to maintain the same n-fold perturbation of a circle as the fastest growing [36,37] mode,

$$Q_n = \frac{\pi\sigma b^2}{6\mu R}(3n^2 - 1), \tag{17}$$

where R is the radius of the bubble. The bubble radius R given by the Bataille formula is plotted as a function of the volumetric pumping rate $q=bQ$ for different n-fold modes in Fig. 2. Conventional pumping with constant Q would appear as a vertical trajectory in Fig. 2. For future experiments one should consider using Park-Homsy pressure jump, $p=-\sigma\kappa\pi/4$, instead of using Bataille's assumption that $p=-\sigma\kappa$.

The particular multifingered pattern that develops depends not only on pumping rate but also on initial perturbations and nonuniformities of the glass plates. In the early stages of the pattern growth, when a bubble begins to deviate from a circle, small unavoidable departures from the circular shape have a greater influence on the development of the interface than the accuracy of pumping or nonuniformities of the glass plates. In practice, we found the smallest m achievable was 5; for smaller target m the growth was too slow to overcome initial perturbations on the bubble's surface before the bubble reached the edge of the cell. We found that although the application of the Bataille formula for small perturbations of a circular bubble is not justifiable for bubbles that have grown large fingers, in practice the Bataille's expression remains helpful in maintaining a symmetrical target pattern.

The present work concerns bubbles that are growing throughout an experiment. If the pumping were stopped, the surface tension would begin to smooth the interfacial regions of high curvature, and an interface could even reverse direction, absorbing the wetting film it left behind.

In most viscous fingering experiments where oil is withdrawn at a constant rate, the process has a natural separation of time scales: $t_Q=A/Q$, determined by pumping rate, is usually much less than the "capillary" time, $t_\sigma=48\mu R^3/(\sigma b^2 n(n+1))$ (for not very high n), which corresponds to smoothing of a pattern by surface tension. The difference between time scales ($t_\sigma \gg t_Q$) makes possible the rich interfacial patterns. However, in our case there is only a single time scale because the pumping Q is adjusted continuously to maintain approximate n-fold symmetry. Equating the scales $t_Q \sim t_\sigma$, one recovers (within a multiplicative factor that depends on n) the Bataille formula. Note that for constant pumping the radius of a bubble is given by $R \sim \sqrt{t}$, while in our case $R \sim \sqrt[3]{t}$ (because $Q \sim 1/R$ and $R^2 \sim Qt$).

C. Image analysis

The oil/air interface in each image was first obtained by subtracting the background image, thresholding, and using an edge detection algorithm. This located the interface to within a pixel. The resolution of the interface was typically 50 pixels/cm, so that one pixel's length was about 0.2 mm.

The position of each point on an interface was then obtained with sub-pixel accuracy by interpolating the location along a line perpendicular to the rough interface that was half of the intensity difference between the inside of the bubble (more intense) and the outside of the bubble (less intense). The algorithm typically found a position of half intensity to 0.1 pixel (about 20 μm, which is small compared to the 125 μm or 384 μm plate separation). This procedure yielded a sufficiently smooth interface so that smoothing was not needed.

D. Determining surface tension

Equation (16) is used to compute the surface tension. The time t_1 is chosen to be when the amplitude a_n [given by Eq. (15)] of the perturbation from a circle exceeds 3 pixels. The time t_2 is chosen so that for slowly growing patterns about 10

images (60 s at 1 frame every 6 s) are collected in t_2-t_1; for rapidly growing patterns about 20 images (10 s at 2 frame/s) are obtained.

The velocity V was calculated by projecting the local normal to the next later good interface. The use of splines allowed for the intersection to occur between interface points, so that the velocity could be computed more precisely. Sums of points of the interface were used as approximations of the contour integrals. The wetting correction (the second integral) contains the capillary number, $Ca=\mu V/\sigma$, which in our experiments was in the range $9\times10^{-5}<\frac{\mu V}{\sigma}<2\times10^{-2}$. This range of Ca is slightly larger than the range that Tabeling and Lichaber observed the 2/3 power law relation of the film thickness [cf. Eq. (13)] [35].

V. RESULTS

A. Harmonic moments

We have calculated the harmonic moments $M_k(t)$ by evaluating the integrals in Eq. (16) for 16 bubbles grown in a cell with a 125 μm gap and for 10 bubbles grown in a Hele-Shaw cell with a 384 μm gap. For each bubble the values of $M_k(t)$ were computed for 50–500 data points spaced at time intervals 0.5–6 s.

We emphasize that our method for determining harmonic moments works well for asymmetric as well as symmetric bubbles. We chose to attempt to develop symmetric bubbles as they grew in order to track accurately the time evolution of particular moments M_k. Hence, for each bubble the pumping rate was adjusted in real time according to Eq. (17), as described in Sec. V B (cf. Figure 2). Most of the bubbles evolved toward a targeted n-fold symmetry, which ranged from fivefold (low-pumping rate) to 14-fold (high-pumping rate). However, some bubbles had an initial shape that was too irregular to evolve into an approximately n-fold bubble during the course of the growth; Fig. 4 is an example of such a bubble.

Our main result is that all observed moments $M_k(t)$ (except M_0) decay in time, as Fig. 3 illustrates. The next subsection presents results confirming that dM_k/dt is proportional to the surface tension σ (neglecting wetting correction) [cf. Eq. (14)], in accord with Richardson's result that all moments are conserved in the zero surface tension case.

B. Test of theory and determination of the surface tension

In the theoretical expression for $M_k(t_2)-M_k(t_1)$, Eq. (16), all quantities can either be determined from our measurements or from independent measurements. Hence, the theory can be directly tested with no adjustable parameters.

We chose to present the test of theory as the ratio of the surface tension deduced from Eq. (16), which we call $\sigma_{measured}$, to the reference value of surface tension measured by the Wilhemy Plate method, $\sigma_{reference}$. Thus surface tension is treated as an unknown whose value can be deduced from Eq. (16), where the integrals and velocity V are determined from analyses of the bubble patterns, while the viscosity μ and gap b are measured independently.

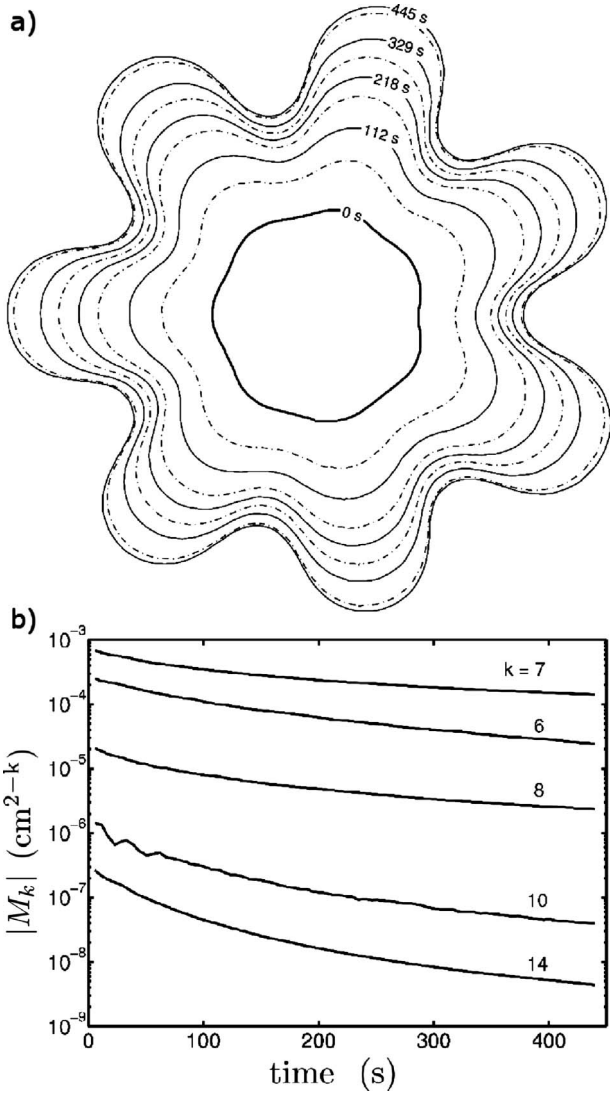

FIG. 3. (a) An air bubble growing in oil in the Hele-Shaw cell (plate separation, 125 μm). Adjacent interfaces are separated by 56 s, and the maximum span of the bubble is 8 cm. The time-dependent pumping rate selects the sevenfold symmetry (cf. Figure 2). (b) Amplitudes of moments 6, 7, 8, 10, and 14, computed using Eq. (6); note that different moments have different units. All moments decay in time, in contrast to the zero surface tension case where the moments are constant.

An example of the results deduced for the surface tension ratio is shown in Fig. 5, which was computed for the nonsymmetric bubble pattern in Fig. 4. For this bubble, the surface tension deduced without a wetting correction is 30% larger than the reference value at short times, where the front velocity is large (see Fig. 4), while at long times the front velocity has become smaller and the difference between the ratios with and without the wetting correction is only a few percent. Further, both ratios are within a few percent of unity, so the value of surface tension deduced from theory is equal to the reference value within the experimental uncertainty.

A measure of the symmetry of a bubble is given by the spectrum of the harmonic moments, i.e., a plot of the normalized moment amplitude, as shown in Fig. 6 for the sym-

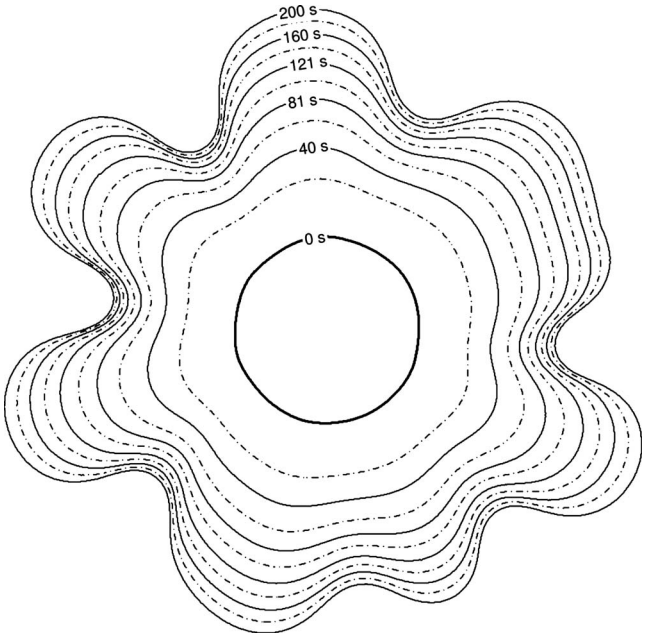

FIG. 4. An air bubble growing without a clean n-fold symmetry. Adjacent interfaces are separated by 20 s.

metric bubble in Fig. 3 and for the nonsymmetric bubble in Fig. 4. The approximately sevenfold bubble in Fig. 3 has a spectrum with significant components at 7, 14, and 21 [Fig. 6(a)], while the nonsymmetric bubble in Fig. 4 has a spectrum with a larger number of significant components, including those at 5, 6, 7, and 8 [Fig. 6(b)].

The mean value for the surface tension $\sigma_{measured}$ was deduced from Eq. (16), including the wetting correction, for each of the 26 bubbles studied, where each bubble was evaluated at 50–500 times during the course of its growth;

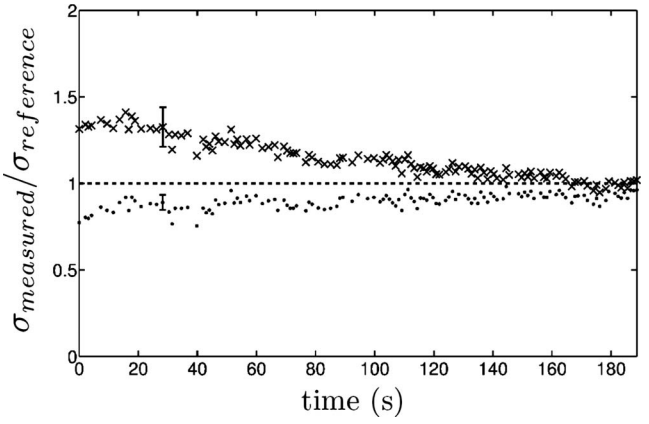

FIG. 5. The ratio of the surface tension value deduced from theory for the data in Fig. 4 to the value independently measured by a traditional method (see text). The upper points ($\times$) are without a wetting correction, and the lower points ($\bullet$) are with the wetting correction in Eq. (16) [the term with the factor 3.8]. The error bars show the standard deviation for each group of points. The value of t_2-t_1 in Eq. (16) was 10 s. The horizontal axis corresponds to t_1.

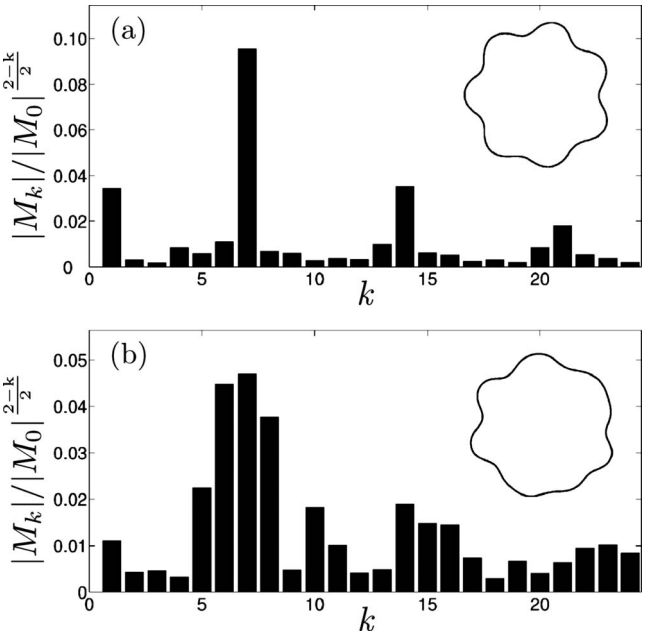

FIG. 6. Spectra of the nondimensional moment amplitudes $|M_k|/|M_0|^{(2-k)/2}$ [Eq. (15)] for two bubbles: (a) A bubble with approximately sevenfold symmetry [Fig. 3(a)], where the main moments are 7, 14, and 21. The moments were calculated at the 112th second of the experiment. (b) A bubble without n-fold symmetry (Fig. 4), where there is a broad spectrum with no dominant moment. The moments were calculated at the 64th second of the experiment.

this involved the numerical evaluation of the integrals in Eq. (16) for more than 6000 data sets. The result is $\sigma_{measured} = 18 \pm 4$ mN/m, where the uncertainty includes both the statistical uncertainty and the estimated systematic uncertainty (see next paragraph). The result for $\sigma_{measured}$ agrees within the experimental uncertainty with $\sigma_{reference} = 21.1 \pm 0.1$ mN/m, determined by the Wilhelmy Plate method. Thus, the theory is quantitatively confirmed within the experimental uncertainty. [If the wetting correction in Eq. (16) is neglected, the result for the surface tension is 23 ± 6 mN/m.] Further, we have examined the dependence of the deduced value of σ on the order of the moment for the accessible moments, $k=5$ to $k=14$, and found no discernible variation with k, nor is there any difference in the value of σ for rapidly grown bubbles, which do not have even approximate k-fold symmetry.

The uncertainty in our result for $\sigma_{measured}$ unfortunately arises in part from a possible systematic error of 9%. The uncertainty in gap thickness (about 4%) contributes significantly to the overall uncertainty. Also, an intermittent problem in camera synchronization could have introduced timing errors in some of the data. Other possible sources of error include the discretization of the integrals and the approximations introduced by the theoretical analysis. The range of applicability of the 2/3 scaling for the film thickness is smaller than the range of Ca produced in our experiments. Another intriguing possible source of error is the 3.8 factor in the wetting correction [34], which has its origin in a numerical integration done in the 1974 Ph.D. Dissertation by Ruschak [38]. If the numerical factor of 3.8 were changed to

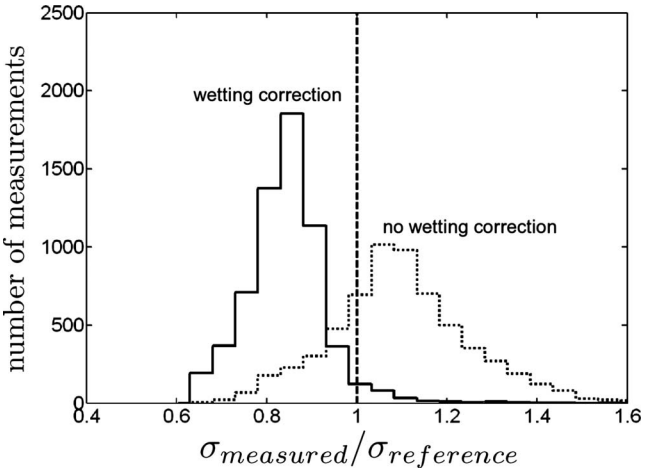

FIG. 7. The distribution of the ratios of surface tension deduced from theory, $\sigma_{measured}$, to $\sigma_{reference}$, determined by the Wilhelmy Plate method. The solid line represents computations that include the wetting term, while the dotted line neglects the wetting correction. The bin size is 0.05. A few outlying points are outside of the abscissa's range.

1.5, then the mean of the distribution in Fig. 7 would correspond to unity. Note that the wetting correction becomes small at long times because the growth velocity V becomes small if the bubbles are grown according to Eq. (17).

The statistics of the results are presented in Fig. 7 as histograms of the ratio $\sigma_{measured}/\sigma_{reference}$, calculated both with and without the wetting correction. The distribution including the wetting correction is narrower because the uncorrected data depend on the pattern growth velocity. The mean value of the ratio with wetting correction is 0.84 ± 0.09 (standard deviation, statistical uncertainty only); the mean value without wetting correction is 1.10 ± 0.1(standard deviation).

Future experiments can straightforwardly reduce the systematic uncertainty. Such experiments should focus on low order moments at intermediate times, to minimize the correction due to wetting without encountering backward motion of the interface.

Bubbles in our experiments were all studied for pumping rates $Q > 0$. Alternatively, one could stop the growth (set $Q = 0$) and observe the relaxation of a bubble. We conducted a few experiments in this way and found that the extracted surface tension values were typically 15%–25% lower than those for growing bubbles. However, for relaxing bubbles the correction for the oil wetting film, which is reabsorbed as the interface retreats, is not known.

VI. DISCUSSION

A. Harmonic moments

We have presented the first demonstration that robust harmonic moments $M_k(t)$ can be deduced from laboratory experiments. Our result for the time derivative of $M_k(t)$ [Eq. (12), or in the form used to compare with experiment, Eqs. (14) and (16)] shows that the moments evolve in time because of nonzero surface tension [Fig. 3(b)]; otherwise all moments except M_0 would be conserved. The harmonic moments are purely geometric quantities [cf. Eq. (6)] and do not involve approximations, fluid properties, or experimental parameters, such as the wetting correction, viscosity, or the gap thickness.

Further, we have derived a relation between the time derivative of the harmonic moments [Eq. (12), or in the form used to compare with experiments, Eq. (16)] and quantities that can all be directly determined by experiment, thus providing a quantitative test of the theory of harmonic moments. The result from measurements on 26 bubbles for two different Hele-Shaw cell gap thicknesses is that theory and experiment agree within the experimental uncertainty (about 20%). This agreement was obtained both on nonsymmetric bubbles and on bubbles with approximate n-fold symmetries varying from 5 to 14. This agreement is robust and, within our experiments, does not depend on how far a bubble has deviated from a circle. Further, we have indicated how it should be straightforward to reduce the experimental uncertainty by an order of magnitude, to test the theory at about a 1% level.

For convenience we have used an expression obtained by Bataille Eq. (17) to adjust the pumping rate $Q(t)$ to grow bubbles that are approximately n-fold symmetric. We find that if an n-fold bubble is grown initially from a slightly perturbed circle, the n-fold symmetry is retained even for large amplitude fingers, far beyond range of applicability of Eq. (17), which was obtained from a linear stability analysis.

B. Implications

Harmonic moments M_k form a complete basis for any complicated time domain D, provided that D is analytic and singly connected. These moments are exceptionally useful for Laplacian growth phenomena such as viscous fingering because all other known representations involve coefficients that change quickly because of instability, thus creating analytic and computational difficulties. In contrast, harmonic moments are free of these problems, no matter how much the domain D deviates from a circle. Loosely speaking, for harmonic moments the whole instability is simply concentrated in the lowest one, M_0 (the area of D).

From a fundamental perspective, the moments M_k for Laplacian growth are exactly the basis that linearizes and "solves" the zero surface tension problem, generating a multitude of exact solutions (summarized in [14]; see also references therein), which are impossible to obtain in any other basis. In this sense, the harmonic moments constitute the most natural basis for Laplacian growth. Our experiments confirm that for nonzero surface tension, the derivative of the moments dM_k/dt is simply proportional to σ (neglecting the wetting correction), so that the zero surface tension limit is smoothly approached. This indicates that the fundamental theoretical results mentioned above, which have been obtained for Laplacian growth theory for the case of zero surface tension, are relevant to real physical systems.

In conclusion, the implications of the demonstration of the harmonic moments description of viscous fingering extends into various branches of mathematical physics (cf. Sec. II) because of the deep connection between Laplacian growth and other problems.

ACKNOWLEDGMENTS

We thank O. Praud for developing the method for maintaining an approximate n-fold symmetry of a bubble (Sec. IV B), and we thank Dmitry Leshchiner for helpful discussions. Acknowledgment is made to the Donors of the American Chemical Society Petroleum Research Fund for support of this research. This work was also supported in part by the LDRD under Grant No. 20070083ER at Los Alamos National Laboratory.

[1] M. C. Cross and P. C. Hohenberg, Rev. Mod. Phys. **65**, 851 (1993).
[2] J. P. Gollub and J. S. Langer, Rev. Mod. Phys. **71**, S396 (1999).
[3] *Dynamics of Curved Fronts*, edited by P. Pelcé (Academic, Boston, 1988).
[4] P. G. Saffman and G. Taylor, Proc. R. Soc. London, Ser. A **245**, 312 (1958).
[5] J. S. Langer, Rev. Mod. Phys. **52**, 1 (1980).
[6] E. Ben-Jacob, Contemp. Phys. **38**, 205 (1997).
[7] H. S. Hele-Shaw, Nature (London) **58**, 34 (1898).
[8] H. Lamb, *Hydrodynamics* (Dover, New York, 1945).
[9] K. A. Gillow and S. D. Howison, (1998), http://www.maths.ox.ac.uk/howison/Hele-Shaw/.
[10] L. Ristroph, M. Thrasher, M. B. Mineev-Weinstein, and H. L. Swinney, Phys. Rev. E **74**, 015201(R) (2006).
[11] *Asymptotics Beyond All Orders*, edited by H. Segur, S. Tanveer, and H. Levine (Plenum, New York, 1991).
[12] M. Mineev-Weinstein, P. B. Wiegmann, and A. Zabrodin, Phys. Rev. Lett. **84**, 5106 (2000).
[13] I. Krichever, M. Mineev-Weinstein, P. Wiegmann, and A. Zabrodin, Physica D **198**, 1 (2004).
[14] M. Mineev-Weinstein, M. Putinar, and R. Teodorescu, J. Phys. A: Math. Theor. **41**, 263001 (2008).
[15] S. Ciliberto and J. P. Gollub, Phys. Rev. Lett. **52**, 922 (1984).
[16] Y. Sawada, A. Dougherty, and J. P. Gollub, Phys. Rev. Lett. **56**, 1260 (1986).
[17] T. A. Witten and L. M. Sander, Phys. Rev. Lett. **47**, 1400 (1981).
[18] N. M. Zubarev, JETP Lett. **94**, 534 (2002).
[19] O. Praud and H. L. Swinney, Phys. Rev. E **72**, 011406 (2005).
[20] D. A. Kessler, J. Koplik, and H. Levine, Adv. Phys. **37**, 255 (1988).
[21] J. S. Langer and H. Müller-Krumbhaar, Acta Metall. **26**, 1681 (1978).
[22] T. C. Halsey, Phys. Today **53**(11), 36 (2000).
[23] S. Richardson, J. Fluid Mech. **56**, 609 (1972).
[24] M. B. Mineev, Physica D **43**, 288 (1990).
[25] P. S. Novikoff, Dokl. Akad. Nauk SSSR **18**, 165 (1938).
[26] P. I. Etingof and A. N. Varchenko, *Why the Boundary of a Round-Drop Becomes a Curve of Order Four* (American Mathematical Society, Providence, RI, 1992), Vol. 3.
[27] J. D. Jackson, *Classical Electrodynamics*, 3rd ed. (Wiley, New York, 1999).
[28] H. J. Landau, *Moments in Mathematics* (American Mathematical Society, Providence, RI, 1987).
[29] B. Gustafsson and M. Putinar, Physica D **235**, 90 (2007).
[30] D. Aharonov and H. S. Shapiro, J. Anal. Math. **30**, 39 (1976).
[31] M. Sakai, *Quadrature Domains*, Lecture Notes in Mathematics (Springer-Verlag, Berlin, 1982), Vol. 934.
[32] G. H. Golub, P. Milanfar, and J. Varah, SIAM J. Sci. Comput. (USA) **21**, 1222 (1999).
[33] B. Gustafsson, C. He, P. Milanfar, and M. Putinar, Inverse Problems **16**, 1053 (2000)
[34] C.-W. Park and G. M. Homsy, J. Fluid Mech. **139**, 291 (1984).
[35] P. Tabeling and A. Libchaber, Phys. Rev. A **33**, 794 (1986).
[36] J. Bataille, Rev. Inst. Fr. Pet. Ann. Combust. Liq. **23**, 1349 (1968).
[37] L. Paterson, J. Fluid Mech. **113**, 513 (1981).
[38] K. J. Ruschak, Ph.D. thesis, University of Minnesota, 1974.